scientific reports

Check for updates

OPEN

Effect of natural aging on biochar physicochemical property and mobility of Cd (II)

Cenwei Liu[1,2], Jing Ye[1,2], Yi Lin[1,2], Xiaomei Wu[3], G. W. Price[4] & Yixiang Wang[1,2]✉

This project utilized both field experiment and laboratory analyses to address the gap in understanding regarding the alterations in properties and functions of biochar, and the impact of heavy metal passivation in soil over long-term natural field aging. The study aimed to examine the changes in the physical and chemical characteristics of biochar over an extended period of natural aging. Additionally, it sought to analyze the impact and mechanisms of biochar in reducing of the harmful effects of the heavy metal cadmium (Cd) during the aging process. Both original and aged biochar conformed to the pseudo-second-order kinetics model and the Langmuir model. The aging process enhanced the adsorption of Cd by biochar and mitigated the leaching of Cd^{2+} into the soil. These findings provide a scientific basis for evaluating biochar's environmental behavior and its potential use in the remediation of soil contaminated with heavy metals.

Keywords Natural aging, Biochar, Adsorption mechanism, Immobilization, Cadmium

Cadmium (Cd) is widely recognized as a prominent hazard associated with heavy metals in soil[1]. Over recent years, agricultural soils have been extensively contaminated by Cd through mining[2] and smelting activities, leading to toxic effects on ecosystems. The high toxicity and environmental persistence of Cd[3] result in irreversible metal accumulation in humans, eventually causing diseases through the food chain[4]. Therefore, the development of environmentally friendly in-situ remediation techniques for Cd pollution is critical. Remediation methods for Cd-contaminated soil are categorized into physical, chemical, and biological technologies, though their field application has been limited[5]. Currently, fixation/stabilization technology is a highly successful remediation approach that significantly decreases the bioavailability of Cd[6].

Biochar, generated through pyrolysis in the presence of limited oxygen, is a carbon-rich solid substance characterized by its porous structure, functional groups, substantial surface area, and low solubility[7,8]. Its use in the remediation of Cd-contaminated soil increased in recent years[9]. According to Huang et al. (2018)[10], biochar can directly immobilize Cd through complexation, precipitation, and cation exchange processes. It also reduces the mobility and bioavailability of Cd in soil by improving soil properties, such as increasing soil pH[11] and altering soil redox potential and microbial composition[12], thereby minimizing Cd uptake by plants[13,14]. Field aging in soil affects biochar due to processes such as water erosion, photocatalysis, and microbial decomposition, altering its structure and physicochemical properties, which in turn, affects its interaction with heavy metals[15,16]. Recent studies have demonstrated the long-term stability of biochar in the remediation of heavy metal-contaminated soil[17,18]. The adsorption mechanisms of aged biochar, including adsorption, complexation, precipitation of surface functional groups with Cd, ion exchange[19], and cation-π interaction[20], remain unchanged. Aging does not activate the adsorbed Cd^{2+} on biochar but promotes the stability of Cd^{2+} adsorbed on its surface[21], primarily through physical changes, increasing the quantity and variety of functional groups on the biochar's surface, and dissolving substances (P, Fe, Ca) inside biochar that can adsorb and precipitate with Cd^{2+}.

The field aging of biochar is a complex and gradual process, making it challenging and time-consuming to study its long-term effects on soil. To circumvent this issue, artificial aging methods such as chemical oxidation and freeze-thaw cycling are currently employed to mimic the natural aging of biochar[22–25], thus accelerating the process. These studies have demonstrated that aging biochar through oxidation reactions enhances its capacity for metal adsorption and immobilization, influencing metal transport and transformation due to alterations in the micro-structure of biochar[25–29]. The surfaces of aged biochar consist of organic molecules combined with inorganic mineral phases, including carbon functional groups containing amino and oxygen. These contribute

[1]Institute of Resources, Environment and Soil Fertilizer, Fujian Academy of Agricultural Sciences, Fuzhou 350003, Fujian, China. [2]Fujian Province Key Laboratory of Agro-Ecological Processes in Hilly Red Soil, Fuzhou 350003, Fujian, China. [3]Institute of Food Science and Technology, Fujian Academy of Agricultural Sciences, Fuzhou 350003, Fujian, China. [4]Faculty of Agriculture, Dalhousie University, Truro, NS B2N 5E3, Canada. ✉email: sd_wolong@163.com

to an expansion of the specific surface area of aged biochar[30,31]. Long-term application of biochar has been shown to enhance soil's Cd capacity, reduce the desorption rate of Cd on soil particle surfaces, and decrease Cd's bioavailability in soil[32]. Therefore, the process of aging can enhance biochar's ability to adsorb heavy metals or decrease the availability of heavy metals.

However, the meta-analysis demonstrated that artificial aging techniques applied to biochar cannot completely replicate the natural aging process that occurs in soil[33]. Chemical oxidation, using agents like concentrated nitric acid and H_2O_2, induces alterations in the surface characteristics of biochar[34]. These alterations primarily involve a rise in the specific surface area and microporosity of biochar, a reduction in pH, and an elevation in oxygen-containing functional groups[35]. However, these chemical treatments lead to a greater level of surface oxidation on aged biochar compared to natural aging. In contrast to natural aging processes, the physical aging method, including freeze-thaw cycling, only induces changes to the porous structure of biochar without significantly altering its elemental composition. Furthermore, research on the adsorption capability of Cd^{2+} by artificially aged biochar reveals contrasting results. For instance, the blocking of soil organic matter is considered to decreases the specific surface area of biochar, while the dissolution of ash and organic matter in biochar may increase it[36].

The field of biochar study is rapidly expanding. Nonetheless, the long-term environmental behaviour of biochar is not as well understood as its short-term remedial efficiency. A crucial question for the effective use of biochar in polluted soils is whether it can maintain effective passivation against heavy metals, particularly during the aging process. Biochar aging is closely connected to alterations in its characteristics, which subsequently impact its ability to absorb Cd^{2+} from the soil. There is a lack of research on the natural aging process of biochar in actual environments, leading to an incomplete understanding of how naturally aged biochar interacts with soil Cd, including heavy metal release characteristics and influencing factors. In particular, there is a scarcity of publications that quantitatively analyze on how the properties of biochar change throughout natural aging and how these changes affect the heavy metal adsorption mechanism. The specifics of these characteristics evolve with aging and the mechanism of Cd adsorption by naturally aged biochar remain unclear. Understanding the relationship between changes in biochar characteristics and its aging process mode could provide theoretical guidance for the long-term use of biochar under natural conditions. Moreover, investigating the precise mechanism by which naturally aged biochar adsorbs and releases soil Cd can offer both theoretical and technical insights into the efficacy of biochar for remedying heavy metal polluted soil. This knowledge can also assist in the management, renewal, and replenishment of biochar. Therefore, this study presents a scientific hypothesis that during the process of natural aging, any changes in the characteristics of biochar may affect the absorption and immobilization of Cd by modifying how soil Cd is adsorbed. This, in turn, could reduce the bioavailability of Cd in the soil.

Materials and methods

Study area

The field experiment was conducted in a tea garden located in Anxi Village, Quanzhou City, Fujian Province, China, which experiences a subtropical monsoon climate. The average annual temperature is 18.5 °C and annual precipitation ranges from 1700 to 1900 mm. The tea garden soil is acidic red soil, characterized by a bulk density of 1.1 g cm^{-3}, a pH of 4.2, total organic carbon (TOC) of 18.9 g kg^{-1}, total nitrogen (TN) of 1.8 g kg^{-1}, available phosphorus of 72.8 mg kg^{-1}, and available potassium of 101.5 mg kg^{-1}. Wheat straw biochar, produced by pyrolysis at 500 °C for 3 h, exhibited a TOC of 470.0 g kg^{-1}, TN of 10.2 g kg^{-1}, alkali-hydrolyzed nitrogen of 24.4 mg kg^{-1}, available phosphorus of 254.2 mg kg^{-1}, ash content of 20.1%, and a pH of 9.3. The biochar was sieved to less than 2 cm and applied to the surface of the test plot, which was then tilled to a depth of 20 cm for thorough mixing in late March 2014, applying a total rate of 40 t ha^{-1} over an area of 15 m^2. No biochar was applied to the control plot (CK). Unapplied biochar samples were sealed and stored in the laboratory, labeled as BC (original biochar).

Soil sample collection and preparation of aging biochar (AB)

In 2022, soil samples were collected from the surfaces layer (0–20 cm depth) of various sites within the tea garden using a manual gouge auger drill. These samples were sieved through a 2 mm sieve, and transferred to a beaker containing a saturated cesium chloride solution with a solution-to-soil ratio of 10:1 (v/w). After homogeneous mixing, the samples were centrifuged at 2500 rpm for 20 min. The supernatant was collected and filtered through an acetate fiber filter membrane. This process, which included the addition of cesium chloride to create a saturated solution for biochar separation and extraction post-centrifugation, was repeated for 3 times[37]. Subsequently, distilled water was added to the mixture, which was then centrifuged at 3500 rpm for 20 min. This step was repeated 3 times to fully remove cesium chloride. The cleaned biochar samples were freeze-dried for 30 h to obtain the separated biochar, labeled as aging biochar (AB).

Determination indexes and methods of BC and AB

The pH of soil samples, both with or without biochar and biochar samples (both original and aged) suspended in water (1:10 w/v) was measured using a pH meter (Mettler Toledo, Switzerland) after a 30-minute equilibrium period. The surface morphology of the original and aged biochar was examined by scanning electron microscopy (SEM, Quanta 250, FEI, Germany), and their specific surface area and pore size were characterized by Brunauer-Emmett-Teller (BET) method (Tristar II 3020, Micromeritics, USA). The crystal structure of biochar was analyzed using an X-ray diffractometer (XRD, D8 Advance, Bruke, Germany) with CuKα radiation[38]. X-ray diffraction patterns were analyzed using Jade 6.5 software. Fourier transform infrared (FTIR) analysis was conducted using a spectrometer (Nicolet iS10, Thermerfey, USA) with OPUS 2.0 software, at a resolution of 2 cm^{-1} and within the wavenumber range of 400 to 4000 $cm^{[-1}$ [39].

Batch adsorption of Cd by biochar

The equilibrium characteristics of Cd^{2+} on both BC and AB were determined using a $Cd(NO_3)_2$ solution in a 0.01 mol L^{-1} $NaNO_3$ background electrolyte. The pH was adjusted to 6.0 using 0.5 mol L^{-1} sodium hydroxide (NaOH) or hydrochloric acid (HCl). The mixture was shaken at 120 rpm at a constant temperature of 25 ℃ for 24 h. Adsorption equilibrium was monitored at various time points, followed by filtration through a 0.45 μm water filtration membrane.

Adsorption isotherms of Cd on both BC and AB were obtained by dissolving of Cd $(NO_3)_2{\cdot}4H_2O$ in double-distilled water to create stock solution of Cd^{2+}. The experiment was conducted in a 50 mL plastic centrifuge tubes, each containing 0.05 g of BC or AB with 25 mL of different concentrations of Cd ranging from 0 to 200 mg L^{-1}. The tubes were shaken at 120 rpm at 25℃ for 24 h, with the pH adjusted to 6.0 at equilibrium. The residual concentration of Cd^{2+} in the filtrates was measured using a flame atomic absorption spectrometer (PE-AA800, USA). Each study was arranged in a randomized design with three replications.

Release kinetic of Cd^{2+} from saturated adsorbed biochar before and after aging

Preparation of biochar with saturated adsorption of Cd

A 0.5 g sample of BC or AB was mixed with 25 ml of a 200 ml L^{-1} Cd $(NO_3)_2{\cdot}4H_2O$ solution, and shaken at 120 rpm at 25℃ for 24 h. The mixture was then centrifuged at 4000 rpm for 30 min, passed through a 0.45 μm filter membrane, and dried at 35 ℃, resulting in samples labeled as BC + Cd and AB + Cd, respectively.

Release kinetic

A 0.05 g sample of BC + Cd or AB + Cd was mixed with 10 mL of 0.1 mol L^{-1} $NaNO_3$ solution (simulating a soil solution environment)[40] and shaken at 200 rpm at 25 ℃ for 24 h. The mixture was then centrifuged at 1500 rpm for 10 min, passed through a 0.45 μm filter membrane, and this process was repeated by adding another 10 mL of 0.1 mol L^{-1} $NaNO_3$ solution to the residual solid. The adsorption-desorption cycles were conducted seven times. The concentration of Cd^{2+} was measured using a flame atomic absorption spectrometer.

Data analysis

The equilibrium adsorption capacity (q_e) and percentage removal (R, %) of BC or AB were calculated as follows:

$$q_e = \frac{(C_0 - C_e)V}{w} \quad (1)$$

$$\mathrm{R}\% = \frac{C_0 - C_e}{C_0} * 100 \quad (2)$$

where C_0 and C_e are the initial and equilibrium concentration of Cd^{2+} (mg L^{-1}), respectively, V (L) is the volume of solution, w(g) is the mass of BC or AB.

The adsorption kinetic data were fitted to Pseudo-first-order and Pseudo-second-order rate expression by the following equations:

Pseudo-first-order: $q_t = q_e(1 - e^{-k_f t})$ (3)

Pseudo-second-order: $q_t = \frac{K_s q_e^2 t}{1 + K_s q_e t}$ (4)

Where q_e and q_t (mg g^{-1}) are the adsorption capacities at equilibrium and time t, respectively. K_f and K_s are the rate constant of the pseudo-first-order and pseudo-second-order kinetic equation, respectively.

Sorption isotherm were analyzed using Langmuir and Freundlich models to quantify the sorption capacity of the BC and AB samples using the following equations:

Langmuir: $Q_e = \frac{Q_m K_L C_e}{1 + K_L C_e}$ (5)

Freundlich: $Q_e = K_F C_e^n$ (6)

where Q_e (mg g^{-1}) is the amount of Cd^{2+} adsorbed at equilibrium, C_e (mg·L^{-1}) is the equilibrium concentration of unadsorbed Cd^{2+}, Q_m is the maximum adsorption capacity (mg g^{-1}), and K_L is Langmuir adsorption characteristic constant (L mg^{-1}). K_F and n are Freundlich constants.

Release kinetics were assessed to study the process of Cd^{2+} release from biochar in a simulated soil environment. The results were fitted with the first-order kinetic equation, the modified Elovich equation, and the double constant rate equation, respectively. The formulas are as follows:

First-order kinetic: $\ln Q_t = a_1 + b_1 t$ (7)

Kinetic Elovich: $Q_t = a_2 + b_2 \ln t$ (8)

Double constant rate: $\ln Q_t = a_3 + b_3 \ln t$ (9)

Where Q_t is the quantity of released heavy metals (mg kg^{-1}) at time t, a and b are constants, and t (h) is the time.

All tests were conducted in triplicates, with error bars in figures representing standard errors. One-way analysis of variance (ANOVA) followed by the Fisher test at a significance level of $p < 0.05$ was used to detect the difference in the sorption capacity of biochar. All data analysis and model fitting were carried out using Microsoft Excel 2010 and Origin 8.0 (OriginLab, Northampton, USA).

Results

Soil properties changes with biochar treatment in tea plantations

The application of biochar significantly influenced the soil pH in the tea plantation. Initially, the soil pH was 4.11. After eight years of biochar application, the soil pH increased by 1.04. In contrast, the soil without biochar treatment showed a slight decrease in pH by 0.07. Soils amended with biochar exhibited substantial

improvements, with TOC and TN increasing by 61.9 and 26.0%, respectively, compared to soils without biochar. This difference in pH values between the soils with and without biochar was statistically significant ($P < 0.05$).

Surface morphological characteristics of BC and AB before and after adsorption Cd^{2+}

The morphological changes in biochar, both in its original state (BC) and after aging (AB), as well as following Cd^{2+} adsorption, were analyzed using scanning electron microscopy (SEM) at 1000x magnification (Fig. 1). The SEM images revealed notable alterations in biochar's surface morphology due to aging. Initially, BC displayed rough asymmetric pores and a sparse distribution of surface pores (Fig. 1a), indicating a more uniform pore distribution.

Upon aging (Fig. 1b), AB predominantly retained its tubular structure without complete collapse. However, the surface structure was partially fragmented and exfoliated, leading to irregularly shaped pores and some damage to the micropore structure. Despite these changes, the overall pore structure remained largely intact. The partial disintegration and thinning of the pore walls, along with the formation of numerous mesoporous structures, contributed to an increased specific surface area. These findings suggest that natural aging, while altering the surface structure of biochar, does not destroy its structural integrity but causes surface splitting.

Further SEM analysis of BC and AB post-Cd^{2+} adsorption revealed that the aperture structure of BC was partly compromised, resulting in a smoother surface. Conversely, the pore structure of AB was nearly destroyed, leading to a much smoother surface. The emergence of granular crystals on the biochar surface after Cd adsorption likely indicates the crystallization of Cd-containing minerals remaining after the adsorption process. Additionally, small particles, likely ash components formed during biochar pyrolysis, were observed adhering to the interior and surface of the pores.

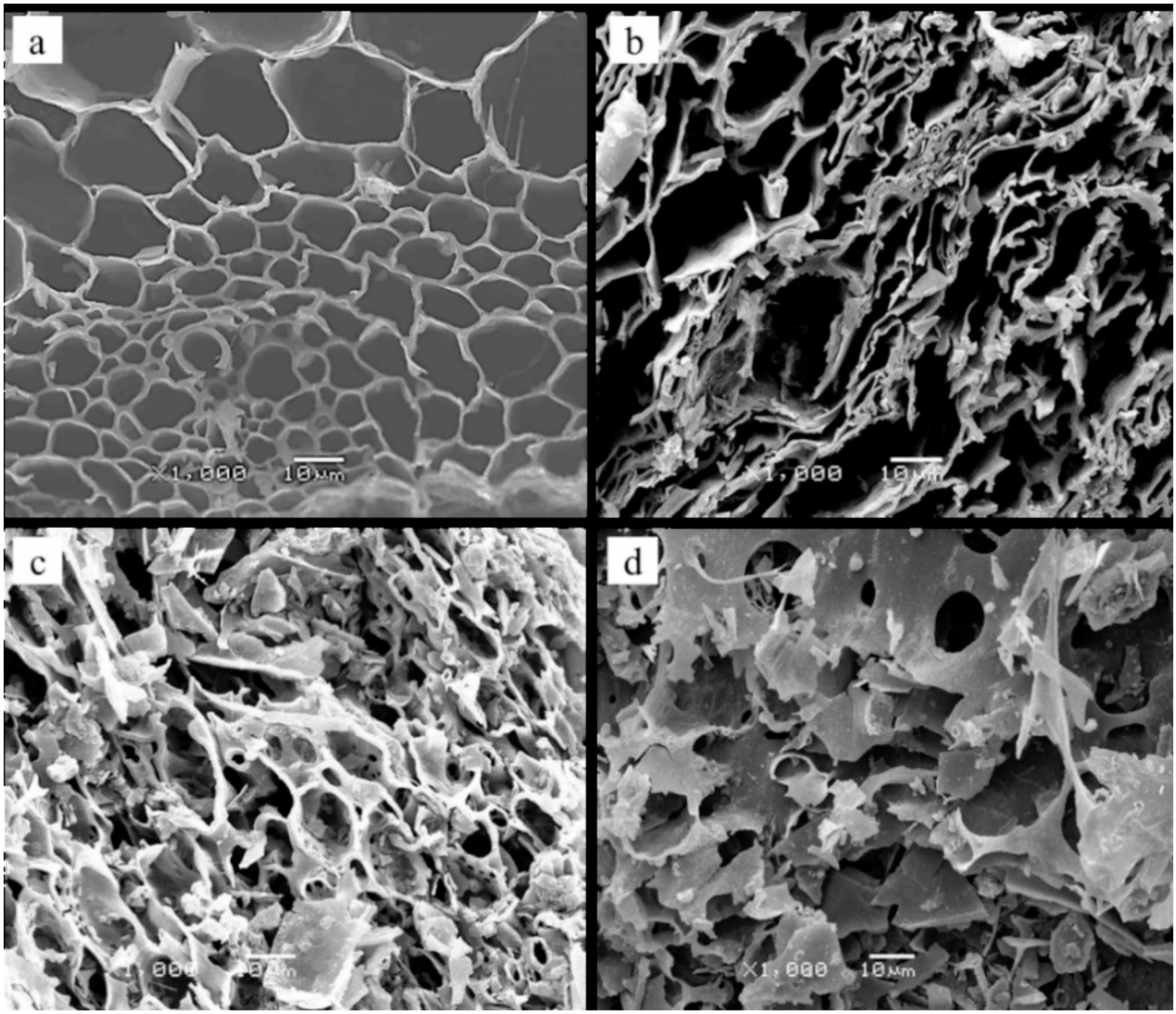

Fig. 1. Scanning electron microscope images of original biochar (a) and aged biochar (b) before adsorption of Cd, and original biochar (c) and aged biochar (d) after adsorption of Cd^{2+}.

	Sample	[a] BET-specific surface area ($m^2\ g^{-1}$)	pore volume ($cm^3\ g^{-1}$)	pore diameter (nm)
Before adsorption	BC	2.9	0.003	2.2
	AB	13.2	0.017	4.6
After adsorption	BC + Cd	45.7	0.046	3.7
	AB + Cd	42.3	0.044	3.8

Table 1. BET analysis of original biochar (BC) and aged biochar (AB) before and after Cd^{2+} adsorption. [a] BET, Brunauer-Emmett-Teller.

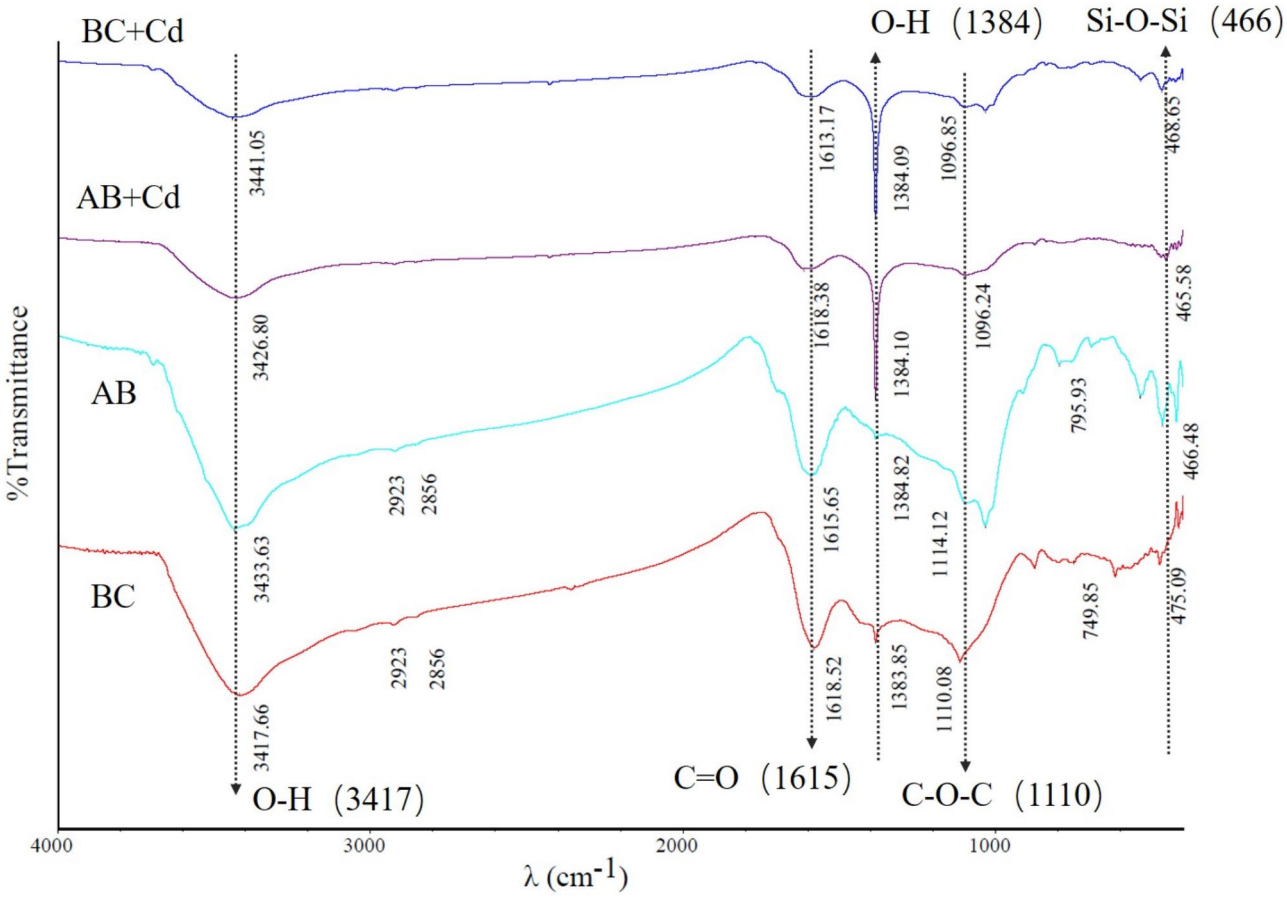

Fig. 2. FTIR spectra of BC and AB before and after adsorption of Cd^{2+} (BC: original biochar; AB: aged biochar before adsorption of Cd^{2+}; BC + Cd: original biochar after adsorption of Cd^{2+}; AB + Cd: aged biochar after adsorption of Cd^{2+}).

BET analysis results of biochar (Table 1) indicated that the specific surface area followed the order: BC + Cd (45.7 $m^2\ g^{-1}$) > AB + Cd (42.3 $m^2\ g^{-1}$) > AB (13.2 $m^2\ g^{-1}$) > BC (2.9 $m^2\ g^{-1}$). After aging, the pore sizes, mesoporous ratio, and specific surface area of biochar increased significantly, with the specific surface area of biochar expanding by 4.6 times compared to the original biochar. This enhancement suggests that the surface properties of biochar are significantly improved post-aging. The natural aging process, driven by fluctuations in temperature and humidity, leads to the deterioration of the micro-pore structure on the biochar surface. Additionally, oxidation promotes the opening of internal pore channels, augmenting the pore structure and providing more adsorption sites for heavy metals, thereby enhancing the physical adsorption capacity of biochar for heavy metals. After adsorption, a large number of Cd oxide particles enriched on the surface increasing the surface area of the biochar.

FTIR spectra characteristics of original and aged biochar

The FTIR spectra of original (BC) and aged biochar (AB) before and after Cd^{2+} adsorption are shown in Fig. 2. The peak patterns of the FTIR spectra for both BC and AB were similar, though the peak intensities differed. The peaks of BC were mainly at wavenumbers of 3417 cm^{-1}, 2923–2856 cm^{-1}, 1618 cm^{-1}, 1384 cm^{-1}, and

466 cm^{-1}. The signals at 3417 cm^{-1} represented –OH stretching vibrations of phenol hydroxyl or lipid groups, primarily arising from biomass carbohydrates[35]. Asymmetric and symmetric stretching vibrations of aliphatic –CH_3 and –CH_2 groups were observed at 2923, 2856 cm^{-1}, respectively[41]. The signals at 1615 cm^{-1} and 1384 cm^{-1} represent C=O stretching vibration in carboxyl group and -OH bending of phenol[42], respectively, and the Si-O symmetric stretching vibration peak of inorganic mineral Si-O-Si was at 466 cm^{-1}. For AB, the prominent peaks were at 3433 cm^{-1} (-OH), 1615 cm^{-1} (C=O), 1384 cm^{-1} (-OH) and 466 cm^{-1} (Si-O-Si). The –OH stretching vibrations increased, and the form and intensity of the signals remained almost unchanged before and after the aging process. An aromatic C-O-C bond was found at 1100 ~ 1260 $cm^{[-1}$ [43], with the peak strength of biochar increasing after natural aging.

The FTIR spectra of BC and AB after Cd^{2+} adsorption showed some differences. The intensity of the peaks for –CH_3 and –CH_2 groups (2923 and 2856 cm^{-1}) followed the order: BC > AB > BC + Cd > AB + Cd, indicating that the content of fatty substances in biochar decreases after aging and Cd^{2+} adsorption. The intensity of the peaks for -COOH and C=O around 1615 cm^{-1} decreased in the order of BC > AB > AB + Cd > BC + Cd. After Cd^{2+} adsorption, the vibration peaks of aromatic O-H (1384 cm^{-1}) were enhanced, suggesting that Cd^{2+} adsorption mainly occurs on the hydroxyl functional group of biochar. The C-H out-of-plane deformation vibration absorption peak of the benzene ring at 763 ~ 787 cm^{-1} in BC and AB was reduced after Cd^{2+} adsorption. In AB, the vibration absorption peak of Si-O-Si near 466 cm^{-1} was significantly enhanced, indicating more pronounced stretching vibration after Cd^{2+} adsorption. The –OH vibration band could be attributed to hydroxyl groups formed upon water adsorption on biochar[44]. The intensity of the –OH vibration band increased after Cd^{2+} adsorption.

XRD analysis of original and aged biochar

The XRD spectra of BC and AB before and after adsorption of Cd^{2+} are shown in Fig. 3. In BC, the peak at 29.5° corresponds to the crystal structure of $CaCO_3$[45]. The strong peak at 26.6° is the characteristic diffraction peak of SiO_2[45], indicating an amorphous carbon structure, along with characteristic diffraction peak of Al_2SiO_5 and $KAlCl_3O_8$. After aging, the characteristic diffraction peak of KCl decreases, primarily showing SiO_2, indicating that aging promotes the formation of inorganic components.

After Cd^{2+} adsorption, $CdCO_3$ and $Cd(OH)_2$ characteristic diffraction peaks were observed in the original biochar, while in the aged biochar, these peaks indicate that during the aging process, the soluble anion CO_2^{3-} can form mineral precipitation with Cd^{2+} along with the oxidation reaction. Previous studies have demonstrated

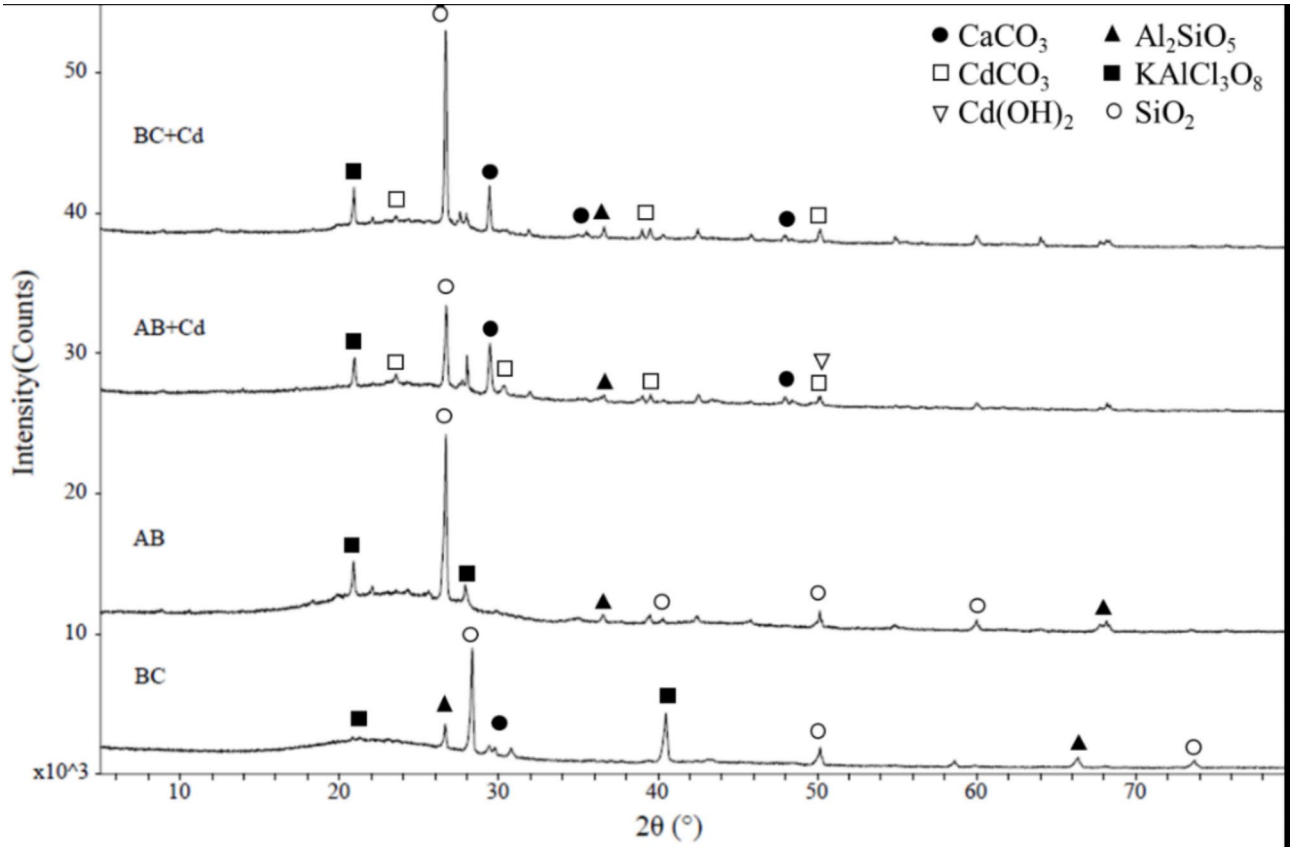

Fig. 3. XRD spectra of BC and AB before and after the adsorption of Cd^{2+} (BC: original biochar; AB: aged biochar before adsorption of Cd^{2+}; BC + Cd: original biochar after adsorption of Cd^{2+}; AB + Cd: aged biochar after adsorption of Cd^{2+}).

that mineral components in biochar can precipitate with Cd^{2+}. Ion exchange has been confirmed as a crucial method for removing heavy metals from biochar, and the presence of $Cd(OH)_2$ in aged biochar suggested that it is abundant in oxygen-containing functional groups and organic carbon. These properties enable the adsorption, complexation, and precipitation of heavy metal Cd with these functional groups, thereby reducing its bioavailability. The data suggest that even as it ages, biochar remains effective in adsorbing Cd from soil, highlighting its potential for long-term use in soil remediation.

Adsorption isotherms, kinetics and desorption of Cd with BC and AB

Adsorption isotherms and adsorption kinetics

Figure 4a shows the effect of initial metal ions concentration (0-200 mg L^{-1}) on adsorption capacity. As the initial ion concentration increased, the adsorption capacity of Cd^{2+} rose to a maximum of 13.6 mg g^{-1} for BC and 14.9 mg g^{-1} for AB, with AB exhibiting a higher capacity than BC. However, when the initial ion concentration increased further, the adsorption capacity of Cd^{2+} decreased to 9.6 mg g^{-1} for BC and 10.4 mg g^{-1} for AB.

The isotherm data from batch sorption experiments were analyzed by using Langmuir and Freundlich models (Fig. 4b) to determine the most suitable model for this study. The calculated values of the Langmuir and Freundlich model parameters are presented in Table 2. The correlation coefficients (R2) for the Freundlich equation were lower than those for the Langmuir equation, suggesting that the Langmuir isotherm provides a better description of Cd^{2+} sorption onto BC and AB. The maximum adsorption capacities (Q_m) for Cd^{2+} indicated that AB had a better adsorption capacity than BC. The theoretical maximum adsorption capacity of Cd^{2+} by naturally aged biochar increased from 15.3 mg g^{-1} before aging to 17.6 mg g^{-1} after aging, an increase of 13.1%. Furthermore, the *n* value obtained from the Freundlich isotherm was higher than 1, indicating favorable adsorption of metal ions on the biochar surface.

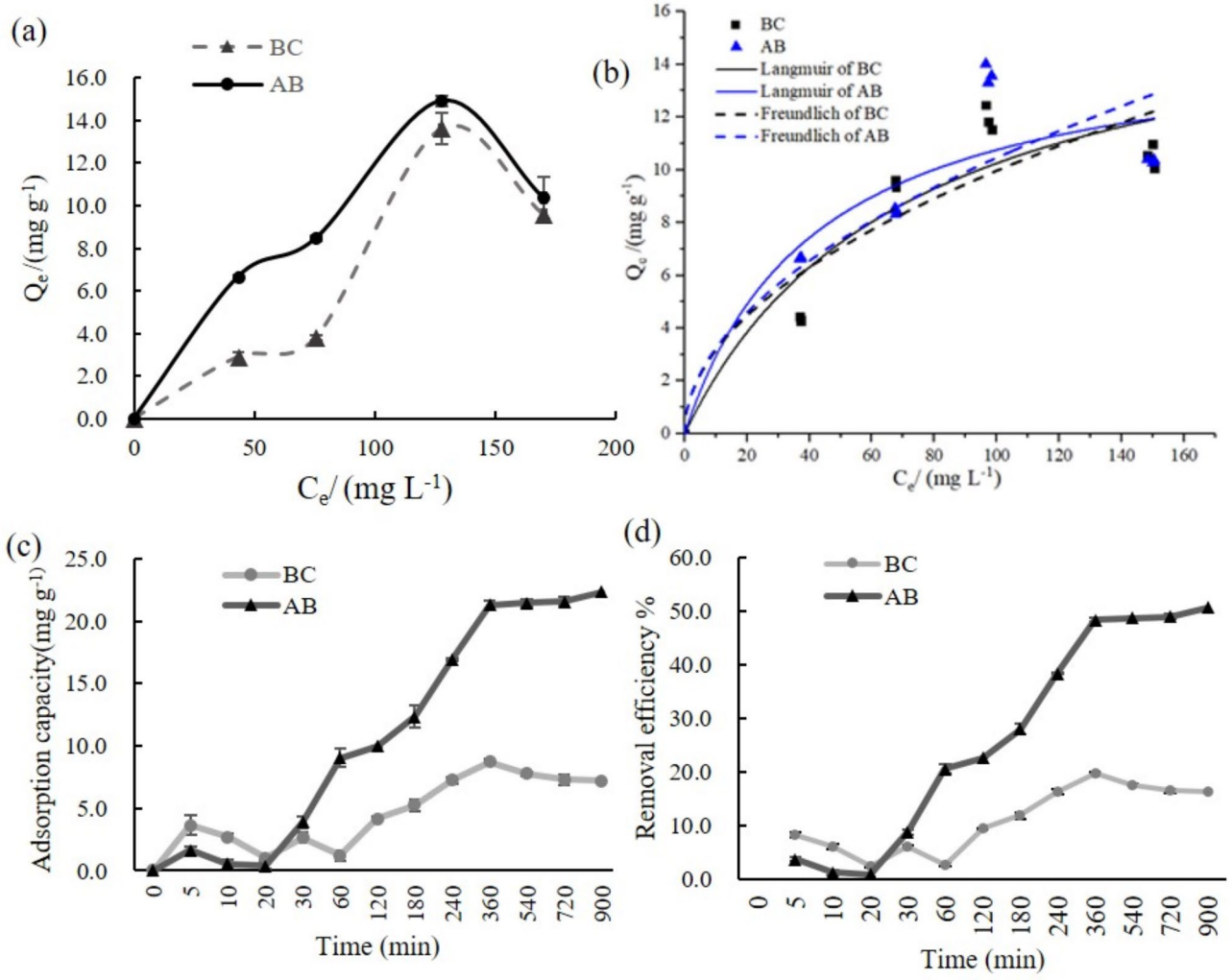

Fig. 4. Effect of the initial Cd^{2+} concentration on the corresponding adsorption isotherms (a); Langmuir and Freundlich adsorption isotherms of Cd^{2+} of original biochar (BC) and aging biochar (AB) (b). Effects of contact time on adsorption capacity and removal percentage of Cd^{2+} of original biochar (BC) (c) and aging biochar (AB) (d).

Material	Langmuir			Freundlich			Pseudo-first-order			Pseudo-second-order		
	Q_m (mg g^{-1})	K_L (mg g^{-1})	R^2	K_F (mg g^{-1})	*n*	R^2	Q_e	K_f	R^2	Q_e	K_s	R^2
BC	15.3	0.01	0.99	0.1	1.1	0.8	8.3 b	0.01	0.80	8.4	0.01	0.85
AB	17.6	0.02	0.99	1.7	2.6	0.9	20.8 a	0.01	0.96	20.8	0.01	0.97

Table 2. Isotherm parameters for adsorption Cd^{2+} onto original biochar (BC) and aging biochar (AB) in aqueous solution fitted from different models.

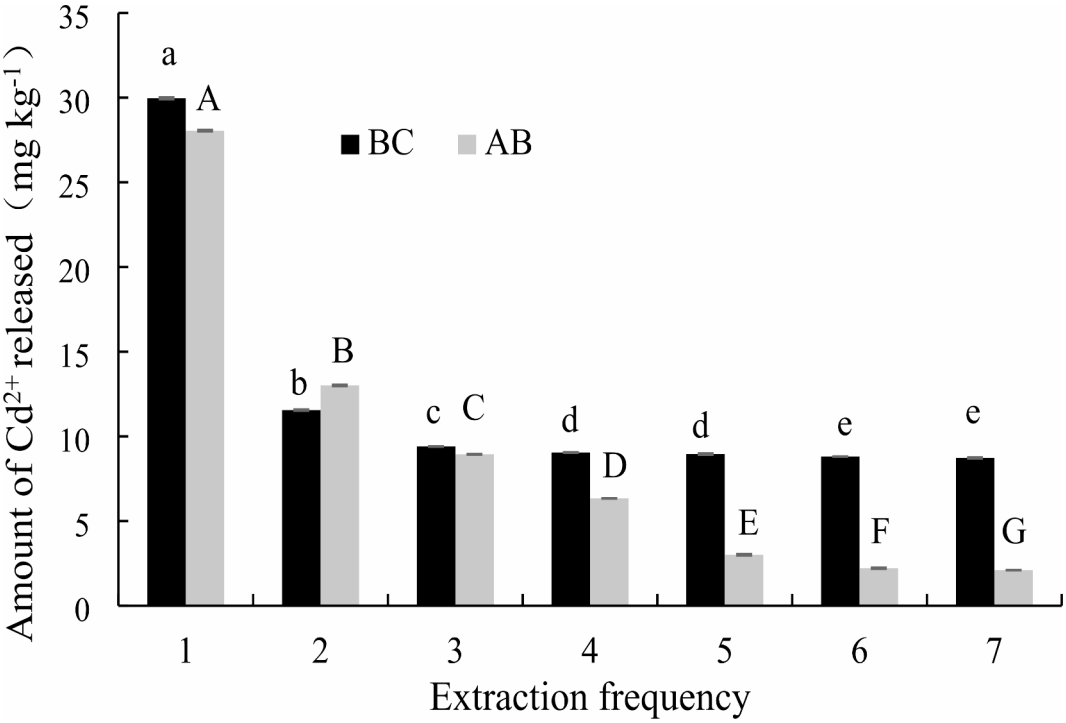

Fig. 5. Effect of extraction frequency on the amount of Cd^{2+} released of original biochar (BC) and aging biochar (AB). Different letters in the same treatment indicate significant difference at 0.05 level.

Biochar	First-order kinetic equation			Modified Elovich Equation			Double constant rate equation		
	a_1	b_1	R^2	a_2	b_2	R^2	a_3	b_3	R^2
BC	3.35	0.17	0.96	24.61	28.54	0.95	3.37	0.54	0.99
AB	3.42	0.12	0.82	28.61	18.74	0.99	3.39	0.42	0.97

Table 3. Elovich kinetic parameters for the extraction of Cd^{2+} on original biochar (BC) and aging biochar (AB).

The effect of contact time on adsorption ability and removal efficiency was analyzed as shown in Fig. 4c and d. The removal efficiency of Cd^{2+} increased with contact time, with rapid adsorption occurring from 20 to 360 min. Equilibrium adsorption capacity was reached at the 360th min for both BC and AB, with minimal changes afterward. AB exhibited a greater adsorption capacity (22.3 mg g^{-1}), 2.8 times higher than BC. A removal efficiency of 50.8% for Cd^{2+} by AB at the 900th min was observed, compared to 19.8% by BC at the 360th min.

The adsorption mechanism of Cd^{2+} onto biochar was investigated using Lagergren pseudo-first order and pseudo-second order equations (Table 2). Maximum adsorption was achieved at the 360th min, after which the capacity decreased. The R^2 of the pseudo-second-order model was higher than that of pseudo-first-order, indicating a better fit with the experimental data for Cd^{2+} ion adsorption.

Immobilization kinetics

The release of Cd from biochar, both before and after aging, was highest at the first extraction, significantly surpassing the release at the second extraction (Fig. 5). As the number of extractions increased, the release of Cd gradually declined, continuing to a lesser extent until the 7th extraction. The quantity of Cd extracted from aged biochar (AB) was generally lower than that from original biochar (BC), with the exception of the second extraction. This suggests that BC has a higher potential for Cd release. Initially, the active acid-soluble heavy metals in biochar rapidly dissolve into the extraction solution. As the reaction progresses, these active heavy metals are depleted, and other, more exchange-resistant forms of heavy metals in biochar are released more slowly.

The cumulative release of heavy metals in biochar (where cumulative release represents the sum of the amount released in the current and all previous extractions) was modeled using a kinetic approach (Table 3). According to the data, the modified Elovich equation effectively simulates the cumulative release behavior of heavy metals from biochar, with an R^2 ranging from 0.82 to 0.99. The b value in the modified Elovich equation represents the release rate of heavy metals in biochar; a higher *b* value indicates a faster release rate. This suggests

that the release mechanism of heavy metals from biochar into the soil environment is not a simple, singular reaction process but rather a complex series of reactions with significant variations in activation energy.

Discussion

Physical and chemical characteristics of biochar after natural aging in soil

Meta-analysis results from Li et al. (2019)[36] suggest that chemical aging significantly reduces the surface area of biochar, while physical aging methods (e.g., freeze-thaw) increase it. In contrast, previous research has shown that the surface area of biochar remains unaffected by natural aging. However, this study found that aging significantly increased the surface area due to structural ruptures caused by surface oxidation[46]. The specific surface area and pore structure of biochar are critical factors determining the efficacy of physical adsorption. An increase in surface area during aging provides additional sites for heavy metal adsorption. Investigations into the isolated simulated aging processes of biochar have shown that physical factors, such as rain erosion, temperature fluctuations, and humidity changes, alter its physical and chemical properties. These changes include a decrease in specific surface area, deterioration of pore structure, reduced pore numbers, and slight acidification[47]. These findings concur with our results, demonstrating that aging affects biochar's acidity and basicity, notably increasing its negative surface charge[48], and thereby enhancing the electrostatic adsorption between biochar and Cd^{2+}. Scanning electron microscopy (SEM) analysis also reflect the surface structure of BC and AB before and after Cd^{2+} adsorption. The images showed a rough porous structure and granular impurities on the biochar surface, indicating that Cd^{2+} has been successfully adsorbed by biochar. The physical properties of biochar surface changed after natural aging, which may have increased the adsorption sites for Cd^{2+}, and facilitated conductive to the oxidation of biochar[49].

These findings were verified by FTIR analysis, which revealed that naturally aged biochar exhibited a greater abundance of C=O and C-O groups. This elevation in oxygen-bearing functional groups in aged biochar compared to the BC is likely due to the oxidation of C-C or C-H bonds during aging[50]. Aging also modifies the prevalence of surface functional groups on the biochar, such as -OH, C=O, and –COOH[35]. The FTIR spectra revealed that AB contained larger amount of oxygen-bearing functional groups than BC, presumably due to the oxidation of C-C or C-H[50]. These groups are thought to strengthen hydrogen bonds and Van der Waals forces between biochar and Cd^{2+} [51]. Other studies reported that biochar possesses abundant oxygen-bearing functional groups (e.g., -OH & -COOH), which can complex with Cd^{2+}[52]. After Cd^{2+} adsorption, the FTIR spectra of aged biochar show shifts of the stretching vibration peaks of -OH and C=O, indicating their interactions with Cd^{2+}. Additionally, a new -COOH stretching vibration peak emerges. The Cd^{2+} adsorption on AB may involve coordination and physical adsorption of Cd^{2+}-π electrons[53], attributable to electrostatic interactions with the aromatic ring of basic carbon. Biochar's aromatic nature aids in Cd^{2+}-π coordination with metal cations acting as electron donors. The appearance of a C=C stretching vibration peak in the FTIR analysis of Cd^{2+} adsorption implies that Cd^{2+}-π electron coordination is an additional adsorption mechanism for aged biochar.

XRD analysis following Cd^{2+} adsorption disclosed new peaks and Cd mineral formation in aged biochar, including $KAlCl_3O_8$, $CdCO_3$, $CaSO_4$, and $Cd(OH)_2$, hinting at the precipitation of $CdCO_3$ subsequent to Cd^{2+} adsorption. These outcomes align with the research of Usman et al. (2016)[54], which proposes Cd adsorption occurs through precipitation, complexation, and ion exchange processes. Typically, metal cations (e.g., K^+, Cd^{2+}, Na^+) adhere to the negatively charged biochar surface via electrostatic interactions, and form complexes with oxygen-containing functional groups on the surface. Biochar may effectively collect Cd^{2+} through ion exchange during the process of adsorption.

Cd^{2+} adsorption and remobilization

The results of biochar adsorption, accurately characterized by the pseudo-second order kinetics, indicate that the adsorbates form a monolayer on the surface of the sorbent and that hydrogen bonding is present[55]. The Langmuir isotherm equation accurately represents the adsorption features of both BC and AB by indicating homogenous adsorption and the formation of a monolayer of Cd^{2+} on the surface of biochar[56]. The sorption of Cd^{2+} was significantly higher in AB compared to BC ($p < 0.05$), indicating that the aging process improves the adsorption characteristics of the biochar. The Cd^{2+} adsorption capacity of biochar typically increases with elevated temperatures and through freeze-thaw aging cycles but may slow or even diminish in the later stages of aging; nevertheless, it remains higher than that of unaged biochar[57].

Both BC and AB demonstrated increased adsorption capacity as the initial concentration of Cd^{2+} ions in solution increased. When the initial concentration exceeded 100 mg L-1, the adsorption capacity of the adsorbents continued to rise until equilibrium was reached, at which point the rate of adsorption equaled the rate of desorption. In contrast, when the initial concentration was below 100 mg L-1, the adsorption capacity increased due to the availability of unoccupied binding sites. As more cadmium ions occupied these sites, the adsorption rate gradually slowed until the adsorbents reached saturation, at which point, no further adsorption could occur, and the adsorbents could no longer accommodate additional cadmium ions[58].

The leaching behavior of heavy metals is likely associated with their morphological distribution within biochar. Initially, soluble heavy metals may leach during the process, but with prolonged extraction, the release of these metals from biochar gradually reduced. For example, the leaching of Cu from biochar tends to stabilize over time[59]. The majority of Cd is released during the first two extraction phases for both BC and AB, with minimal subsequent release from AB. In contrast, BC continues to release Cd. This pattern suggests that active, acid-soluble heavy metals in biochar are quickly solubilized in the early stage of reaction. As the reaction progresses, the readily available metals are depleted, and the release of more leaching-resistant forms occurs gradually[60,61].

Conclusion

Aging of biochar in natural fields entails a complex array of processes. While artificial aging can simulate natural biochar aging, it cannot fully replicate every aspect of the aging that occurs in soil environments. Field studies of natural aging provide deeper insights into the effectiveness of biochar in adsorbing heavy metals. The aging of biochar can have both beneficial and adverse effects on sustainable agriculture. On the positive side, it supports the sustained, slow release of nutrients, contributing to long-term soil fertility. Additionally, enhanced surface complexation aids in the prolonged immobilization of potentially toxic metals within the soil, underscoring biochar's value in environmental remediation efforts.

Data availability

Data provided in a supplementary file.

Received: 24 May 2024; Accepted: 10 September 2024
Published online: 27 September 2024

References

1. Mostofa, M. G. et al. Interactive effects of salicylic acid and nitric oxide in enhancing rice tolerance to cadmium stress. *Int. J. Mol. Sci.* **22**, 5798 (2019).
2. Taati, A., Salehi, M. H., Mohammadi, J., Mohajer, R. & Díez, S. Pollution assessment and spatial distribution of trace elements in soils of Arak industrial area, Iran: Implications for human health. *Environ. Res.* **187**, 109577 (2020).
3. Maity, S. et al. Oxidative stress responses of two different ecophysiological species of earthworms (Eutyphoeus waltoni and Eisenia fetida) exposed to Cd-contaminated soil. *Chemosphere***203**, 307–317 (2018).
4. Wang, H. R. et al. The multiple effects of hydrogen sulfide on cadmium toxicity in tobacco may be interacted with CaM signal transduction. *J. Hazard. Mater.***403**, 123651 (2021).
5. Liu, M. et al. A critical review of biochar-based materials for the remediation of heavy metal contaminated environment: Applications and practical evaluations. *Sci. Total Environ.***806**, 150531 (2022).
6. Sun, J. et al. Effects of biochar on cadmium (cd) uptake in vegetables and its natural downward movement in saline-alkali soil. *Environ. Pollut. Bioavail.***1**, 36–46 (2020).
7. Leng, L. et al. An overview on engineering the surface area and porosity of biochar. *Sci. Total Environ.***763**, 144204 (2021).
8. Liu, Y. et al. Impact of biochar amendment in agricultural soils on the sorption, desorption, and degradation of pesticides: A review. *Sci. Total Environ.***645**, 60–70 (2018).
9. Sugawara, K. et al. Effects of pyrolysis temperature and chemical modification on the adsorption of cd and as (V) by biochar derived from pteris vittata. *Int. J. Environ. Res. Public Health***9**, 5226 (2022).
10. Huang, F. et al. Quantitative contribution of Cd^{2+} adsorption mechanisms by chicken-manure-derived biochars. *Environ. Sci. Pollut Royal***25**, 28322–28334 (2018).
11. Lu, H. et al. Effects of the increases in Soil pH and pH buffering capacity induced by crop residue biochars on available cd contents in acidic paddy soils. *Chemosphere (Oxford)***301**, 134674 (2022).
12. Cheng, C. et al. Combined biochar and metal-immobilizing bacteria reduces edible tissue metal uptake in vegetables by increasing amorphous Fe oxides and abundance of Fe-and Mn-oxidising Leptothrix species. *Ecotox Environ. Safe*. **206**, 111189 (2020).
13. Yuan, C. et al. A meta-analysis of heavy metal bioavailability response to biochar aging: Importance of soil and biochar properties. *Sci. Total Environ.* **756**, 144058 (2021).
14. Bashir, S. et al. Role of sepiolite for cadmium (cd) polluted soil restoration and spinach growth in wastewater irrigated agricultural soil. *J. Environ. Manage.* **258**, 110020 (2020).
15. O'Connor, D. et al. Biochar application for the remediation of heavy metal polluted land: A review of in situ field trials. *Sci. Total Environ.* **619**, 815–826 (2018).
16. Duan, W. et al. Environmental behavior of engineered biochars and their aging processes in soil. *Biochar***4**, 339–351 (2019).
17. Gao, R. et al. Remediation of Pb, Cd, and Cu contaminated soil by co-pyrolysis biochar derived from rape straw and orthophosphate: Speciation transformation, risk evaluation and mechanism inquiry. *Sci. Total Environ.***730**, 139119 (2020).
18. Zhao, M. et al. Mechanisms of pb and/or zn adsorption by different biochars: biochar characteristics, stability, and binding energies. *Sci. Total Environ.***717**, 136894 (2020).
19. Xu, D. et al. Mechanisms of cadmium adsorption by ramie nano-biochar with different aged treatments. *Appl. Soil. Ecol.***193**, 105175 (2024).
20. Jing, F., Sohi, S. P., Liu, Y. & Chen, J. Insight into mechanism of aged biochar for adsorption of PAEs: reciprocal effects of ageing and coexisting Cd^{2+}. *Environ. Pollut.***242**, 1098–1107 (2018).
21. Xie, Y. et al. Study on the physicochemical properties changes of field aging biochar and its effects on the immobilization mechanism for Cd^{2+} and Pb^{2+}. *Ecotox Environ. Safe*. **230**, 113107 (2022).
22. Chen, X. et al. Three-year field experiments revealed the immobilization effect of natural aging Biochar on typical heavy metals (Pb, Cu, cd). *Sci. Total Environ.***912**, 169384 (2024).
23. Lebrun, M. et al. Natural ageing of biochar improves its benefits to soil pb immobilization and reduction in soil phytotoxicity. *Environ. Geochem. Health***8**, 6109–6135 (2023).
24. Wang, L. et al. Biochar aging: Mechanisms, physicochemical changes, assessment, and implications for field applications. *Environ. Sci. Technol.***23**, 14797–14814 (2020).
25. Yang, K. et al. Enhanced immobilization of cadmium and lead adsorbed on crop straw biochars by simulated aging processes. *Environ. Pollut.***302**, 119064 (2022).
26. Meng, Z. et al. Transport and transformation of cd between biochar and soil under combined dry-wet and freeze-thaw aging. *Environ. Pollut.***263**, 114449 (2020).
27. Tan, X. F. et al. One-pot synthesis of carbon supported calcined-Mg/Al layered double hydroxides for antibiotic removal by slow pyrolysis of biomass waste. *Sci. Rep.* **1**, 39691 (2016).
28. Cui, H. et al. Aging reduces the bioavailability of copper and cadmium in soil immobilized by biochars with various concentrations of endogenous metals. *Sci. Total Environ.* **797**, 149136 (2021).
29. Yang, K. et al. Effect of aging on stabilization of cd and ni by biochars and enzyme activities in a historically contaminated alkaline agricultural soil simulated with wet–dry and freeze–thaw cycling. *Environ. Pollut.***268**, 115846 (2021).
30. Dong, X., Li, G., Lin, Q. & Zhao, X. Quantity and quality changes of biochar aged for 5 years in soil under field conditions. *Catena***159**, 136–143 (2017).
31. Joseph, S. et al. Microstructural and associated chemical changes during the composting of a high temperature biochar: Mechanisms for nitrate, phosphate and other nutrient retention and release. *Sci. Total Environ.***618**, 1210–1223 (2018).
32. Kamran, M. et al. Biochar alleviates cd phytotoxicity by minimizing bioavailability and oxidative stress in pak choi (Brassica chinensis L.) cultivated in Cd-polluted soil. *J. Environ. Manage.***250**, 109500 (2019).

33. Kong, L. L. et al. Biochar: an effective amendment for remediating contaminated soil. *Rev. Environ. Contam. T.***228**, 83–99 (2013).
34. Fan, Q. et al. Effects of chemical oxidation on surface oxygen-containing functional groups and adsorption behavior of biochar. *Chemosphere***207**, 33–40 (2018).
35. Mia, S. et al. Aging induced changes in biochar's functionality and adsorption behavior for phosphate and ammonium. *Environ. Sci. Technol.***15**, 8359–8367 (2017).
36. Li, H. et al. How close is artificial biochar aging to natural biochar aging in fields? A meta-analysis. *Geoderma***352**, 96–103 (2019).
37. Chi, J. et al. A method for separation of biochar from soil and its application. Chinese: CN 110964582A, 2020-04-07. (2020).
38. Bashir, S. et al. Efficiency and surface characterization of different plant derived biochar for cadmium (cd) mobility, bioaccessibility and bioavailability to Chinese cabbage in highly contaminated soil. *Chemosphere (Oxford)***211**, 632–639 (2018).
39. Chen, Y. et al. The impact of pyrolysis temperature on physicochemical properties and pulmonary toxicity of tobacco stem micro-biochar. *Chemosphere (Oxford)***263**, 128349 (2021).
40. Sosa-Rodríguez, Fabiola, S. et al. Sphalerite oxidation simulating acidic, circumneutral and alkaline conditions to account for weathering behavior and Zn release. *J. Geochem. Explor.* **247**, 107163 (2023).
41. Chen, Z., Chen, B. & Chiou, C. Fast and slow rates of naphthalene sorption to biochars produced at different temperatures. *Environ. Sci. Technol.* **46**, 11104–11111 (2012).
42. Ghaffar, A. et al. Effect of biochar aging on surface characteristics and adsorption behavior of dialkyl phthalates. *Environ. Pollut.206*, 502–509 (2015).
43. Wang, S. J. et al. Lead and uranium sorptive removal from aqueous solution using magnetic and nonmagnetic fast pyrolysis rice husk biochars. *RSC Adv.***8**, 13205 (2018).
44. Adilina, I. B. et al. Understanding the surface characteristics of biochar and its catalytic activity for the hydrodeoxygenation of guaiacol. *Catalysts***12**, 1434 (2021).
45. Wang, R. et al. Investigating the adsorption behavior and the relative distribution of Cd^{2+} sorption mechanisms on biochars by different feedstock. *Bioresour Technol.***261**, 265–271 (2018).
46. Nie, T. et al. Effect of biochar aging and co-existence of diethyl phthalate on the mono-sorption of cadmium and zinc to biochar-treated soils. *J. Hazard. Mater.***408**, 124850 (2021).
47. Chen, H. et al. Effect of biochars on the bioavailability of cadmium and di-(2-ethylhexyl) phthalate to Brassica chinensis L. in contaminated soils. *Sci. Total Environ.***678**, 43–52 (2019).
48. Atiah, K. et al. Changes in bulk and surface properties of two biochar types during 12 months of field ageing in two West-African soils. *West. Afr. J. Appl. Ecol.***28**, 61 (2020).
49. Sigmund, G. et al. Small biochar particles hardly disintegrate under cryo-stress. *Geoderma***430**, 11632 (2023).
50. Tan, L. et al. Effect of three artificial aging techniques on physicochemical properties and pb adsorption capacities of different biochars. *Sci. Total Environ.***699**, 134223 (2020).
51. Liu, Y. et al. Oxidative ageing of biochar and hydrochar alleviating competitive sorption of Cd (II) and Cu (II). *Sci. Total Environ.***725**, 138419 (2020).
52. Qu, J. et al. Iron/Manganese bnary metal oxide-biochar nano-composites with high adsorption capacities of Cd^{2+}: Preparation and adsorption mechanisms. *J. Water Process. Eng.***51**, 103332 (2023).
53. Zhu, L. et al. Key factors and microscopic mechanisms controlling adsorption of cadmium by surface oxidized and aminated biochars. *J. Hazard. Mater.***382**, 121002 (2020).
54. Usman, A. et al. Sorption process of date palm biochar for aqueous Cd (II) removal: efficiency and mechanisms. *Water Air Soil. Pollut* **227**, 1–16 (2016).
55. Shin, K. Y. et al. Heavy metal ion adsorption behavior in nitrogen-doped magnetic carbon nanoparticles: isotherms and kinetic study. *J. Hazard. Mater.* **1**, 36–44 (2011).
56. Zhou, N. et al. Effect of pyrolysis condition on the adsorption mechanism of heavy metals on tobacco stem biochar in competitive mode. *Environ. Sci. Pollut. Royal* **26**, 26947–26962 (2019).
57. Yin, G. et al. Novel Fe-Mn binary oxide-biochar as an adsorbent for removing cd (II) from aqueous solutions. *Chem. Eng. J.* **389**, 124465 (2020).
58. Farooq, U. et al. Biosorption of heavy metal ions using wheat based biosorbents–a review of the recent literature. *Bioresour Technol.* **14**, 5043–5053 (2010).
59. Dai, Z. et al. Speciation analysis and leaching behaviors of selected trace elements in spent SCR catalyst. *Chemosphere* **207**, 440–448 (2018).
60. Du, J. et al. Research on thermal disposal of phytoremediation plant waste: Stability of potentially toxic metals (PTMs) and oxidation resistance of biochars. *Process. Saf. Environ.* **125**, 260–268 (2019).
61. Park, J. H. et al. Cadmium adsorption characteristics of biochars derived using various pine tree residues and pyrolysis temperatures. *J. Colloid Interface Sci.* **553**, 298–307 (2019).

Author contributions

C.L. wrote the main manuscript text and funding acquisition; J.Y. worked on the data calculation; Y. L. worked on data analysis; X. W. worked on Formal analysis, and prepared Fig. 1; G.W.P. took charged in review & editing of the manuscript; Y.W. was supervision, project administration and corresponding author. All authors have reviewed and agreed to the published version of the manuscript.

Funding

This research was funded by the Fujian Natural Science Foundation project (Grant No. 2022J01447); Fujian Province Public Welfare Scientific Research Program (Grant No. 2023R1062); the Central Government Guided Local Science and Technology Development projects (Grant No. 2023L3022).

Declarations

Competing interests

The authors declare no competing interests.

Additional information

Supplementary Information The online version contains supplementary material available at https://doi.org/10.1038/s41598-024-72771-8.

Correspondence and requests for materials should be addressed to Y.W.